Wire scanners in low energy accelerators

P. Elmfors [1], A. Fassò [2], M. Huhtinen, M. Lindroos, J. Olsfors and U. Raich

CERN, Geneva, Switzerland

Fast wire scanners are today considered as part of standard instrumentation in high energy synchrotrons. The extension of their use to synchrotrons working at lower energies, where Coulomb scattering can be important and the transverse beam size is large, introduces new complications considering beam heating of the wire, composition of the secondary particle shower and geometrical consideration in the detection set-up. A major problem in treating these effects is that the creation of secondaries in a thin carbon wire by a energetic primary beam is difficult to describe in an analytical way. We are here presenting new results from a full Monte Carlo simulation of this process yielding information on heat deposited in the wire, particle type and energy spectrum of secondaries and angular dependence as a function of primary beam energy. The results are used to derive limits for the use of wire scanners in low energy accelerators.

---

[1] Present address: University of Stockholm, Fysikum, Box 6730, S-113 85 Stockholm, Sweden
[2] Present address: Stanford Linear Accelerator Center, Radiation Physics department, ms 48, P.O. Box 4349, Stanford CA 94309, USA
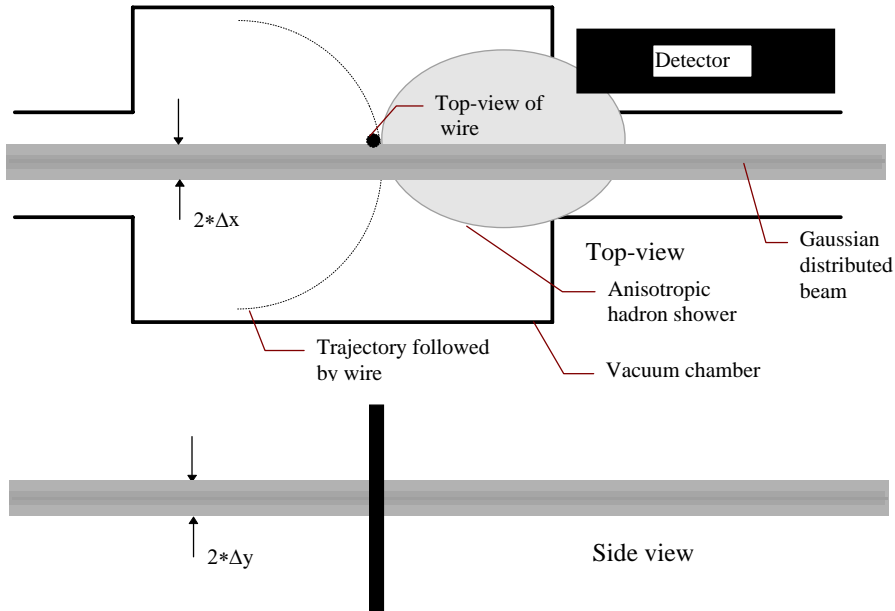
Fig. 1. Geometry of beam and wire

1 Introduction

Fast wire scanners have been used successfully for beam profile measurements in the CERN-PS [1–5] for more than ten years. We are presently considering to extend the use of them to the PS injector, the PS Booster. The PSB is a synchrotron with four superimposed rings accelerating up to 1×10^{13} protons per ring from 50 MeV to 1 GeV kinetic beam energy. Operation of the fast wire scanners in this low energy region where the physical beam emittance is large has triggered us to take a new look at the theory for wire heating, emittance blow up and the importance of the geometrical relationships in the detector set-up. The work has been specially aimed at the low energy domain of a proton beam but the results are in general valid also for the high energy domain.

The design and operation of fast wire scanners has been described elsewhere [1–8]. We will here only concern ourselves with the problems that set the limits for the use of these devices. For our discussion we need to define a geometry and as a starting point we use the geometry shown in Fig. 1. The figure is showing an instant in the process of the wire sweeping through the beam. The transverse particle distribution within the beam is for simplicity taken to be Gaussian. As a measure for the beam size we have in this work used $4 \times \sigma$ of the Gaussian beam profile as the measure for the beam width. This transforms to the so called 2σ emittance which at the CERN-PS is the standard quoted measure for transverse beam emittance.

2 Simulation of beam-wire interaction

The fast wire scanner method for measuring beam profiles is based on the simple fact that an energetic particle beam passing any obstacle , in our case a thin carbon wire, will create a secondary particle shower which is proportional to the primary beam intensity. The limits for the method is determined by how much deposited heat the carbon wire can support and the possibility of detecting the secondary particles. With this in mind we have simulated the process of a primary proton beam passing a thin carbon wire using the FLUKA code, [9]. The main interaction parameters studied are the heat deposited in the carbon wire, the angular dependence of the particle shower as a function of energy and the particle composition and energy spectrum of the secondaries.

2.1 Heat deposited in the carbon wire

The simulation was especially aimed at calculating the part of the interaction energy deposited in the wire (which eventually is transferred to heat). The fraction of the total deposited energy leaving through the nuclear interaction proved to be very small, e.g. at 100 MeV kinetic beam energy 35.5 keV is deposited in wire as heat and only 0.67 keV is leaving the wire through the nuclear interaction. The nuclear interaction part of the energy remains more or less constant up to the highest simulated value at 1 GeV. Furthermore, we also calculated the possible spread of the deposited energy along the wire due to internal scattering and even at the finest spatial resolution used in our simulations of 0.001 mm no significant smearing of the deposited energy was observed.

As a model for the energy loss we take the Bethe–Bloch formula (see e.g.[12])

$$\frac{dE}{dz} = 2\pi N_a r_e^2 m_e c^2 \rho \frac{Z}{A} \frac{z^2}{\beta^2} \left[\ln\left(\frac{2m_e c^2 \beta^2 \gamma^2 W_{\max}}{I^2} \right) - 2\beta^2 \right] \quad , \tag{1}$$

The symbols are explained in Tab. 1. The maximum energy transfer can be written as

$$W_{\max} = \frac{2m_e c^2 \beta^2 \gamma^2}{1 + 2s\gamma + s^2} \quad . \tag{2}$$

with $s = m_e/m_p$. The details of the notation is explained in e.g. [12]. For protons in the beam s is small and we can approximate

$$W_{\max} \simeq 2m_e c^2 \beta^2 \gamma^2 \quad , \tag{3}$$

unless $2s\gamma \gtrsim 1$, i.e. the energy of the proton beam is more than about 2 TeV.

Table 1
Numerical values used in the Bethe–Bloch equation for a carbon wire.

|			
N_a	Avogadros Number	6.022×10^{26}	$\times 10^{-3} \mathrm{mol}^{-1}$
r_e	classical electron radius	2.817×10^{-15}	m
m_e	electron rest mass	9.109×10^{-31}	kg
c	light velocity	2.9979×10^{8}	$\mathrm{m\,s}^{-1}$
ρ	graphite density	1.77×10^{3}	$\mathrm{kg\,m}^{-3}$
Z	atomic number	6	
A	atomic weight	12	
z	charge of incident particle	1	
W_{max}	maximum energy transfer	$1.637 \times 10^{-13} \beta^2 \gamma^2$	$\mathrm{kg\,m^2\,s}^{-2}$
m_p	mass of incident particle	1.672×10^{-27}	kg
I	mean excitation potential	1.266×10^{-17}	$\mathrm{kg\,m^2\,s}^{-2}$
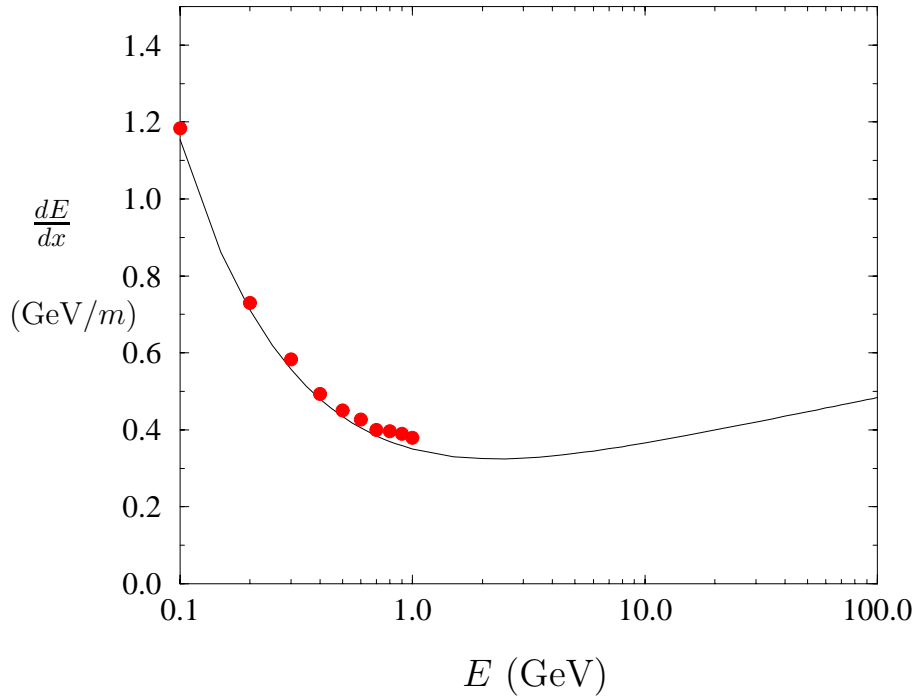
Fig. 2. Simulated and Bethe–Bloch values of dE/dz for a carbon wire as a function of kinetic energy , $E = m_p c^2 (\gamma - 1)$.

The values we use in the Bethe–Bloch equation are compiled in Tab. 1 and the values wire together with other numerical values are given in Tab. 2.

In Fig. 2 we compare the Bethe–Bloch equation with the Monte–Carlo simulation. The deviation between the theory and the simulation is small and

4

Table 2
Additional accelerator, beam and wire parameters

η	emissivity (C)	0.88	
σ	Stephan–Boltzmann constant	5.67×10^{-8}	$\mathrm{kg\,s^{-3}\,K^{-4}}$
c_V	heat capacity (C)	1.25×10^{6}	$\mathrm{kg\,s^{-2}\,m^{-1}\,K^{-1}}$
r	wire radius	1.5×10^{-5}	m
N	number of beam particles	2×10^{13}	
τ_0	revolution time at $\beta=1$	2.1×10^{-6}	s
ϵ_{Nx}	normalised beam emittance, x	1.7×10^{-4}	m
ϵ_{Ny}	normalised beam emittance, y	9.0×10^{-5}	m
β_{Tx}	Twiss value, x	12	m
β_{Ty}	Twiss value, y	21	m
v	wire velocity	20	$\mathrm{m\,s^{-1}}$
κ	heat conductivity (C)	150	$\mathrm{W\,m^{-1}K^{-1}}$

justifies using the Bethe–Bloch equation for the rest of the analysis.

2.2 Secondary particle shower

The inelastic cross section of a 100 MeV proton in carbon is of the order of 240 mb, rising to about 250 mb at 1 GeV. The elastic cross section drops from about 180 mb at 100 MeV to roughly 100 mb at 1 GeV.

For the typical total scattering cross section of 400 mb and a carbon density of $2.3\mathrm{g/cm^3}$ the mean free path in the wire material is 21.7 cm. For a wire with a radius of $15\,\mu$m the average number of protons needed to obtain one scattering is 9200. Since the interaction probability is so small, scattering of the produced secondaries can be neglected.

Using the scattered particles the beam intensity can be monitored, by measuring the energy deposition in a detector well away from the beam axis. This requires that the energy deposited per one scattered particle is known. This can be calculated with the FLUKA Monte Carlo program [9].

The simulations should be carried out in a realistic geometry, since stray radiation around an accelerator may give a significant contribution to the total energy deposition. The simulations presented in the following were carried out in a very idealized geometry.

The detectors were represented by polyethylene disks of 5 mm thickness, 3 cm diameter and a density of $0.95\,\mathrm{g/cm^3}$. These were placed at a radial distance

of 50 cm from the point where the beam hits the wire. 17 detectors, starting at a polar angle of 10 degrees and spaced by 10 degrees were used.

The scattering of protons with 100 MeV and 1 GeV kinetic energy was studied. Instead of simulating a beam hitting the wire, we first created sets of 10000 elastic and 10000 inelastic events for both energies. The secondaries from these events were then mixed in ratios given by the inelastic and elastic cross sections. Since these event sets were postulated to be representative of an infinite number of events, the event structure itself was not important. So the azimuth angle of each secondary particle could be separately sampled between zero and 2π. Due to the small solid angle covered by the detectors the relatively limited number of events could be reused several times to improve the statistics of the quantities scored at the detectors.

The obtained energy deposition is shown in Fig. 3. Normalization is to one proton incident on the wire assuming a circular wire with $30\,\mu$m diameter. In the upper plots the total energy deposition and the fraction coming from elastic scattering is shown separately. It can be seen that the elastic contribution quickly becomes negligible, which is fortunate, since the angular distributions of the elastic scattering in FLUKA are not really optimized to reproduce single scattering distributions. In particular they lack the diffractive structure, which is characteristic for elastic scattering and only reproduce rough trends of the differential cross section.

The lower plots show a comparison of the energy deposition in the detectors if material is introduced between the wire and the detectors. In a real situation there will always be at least a thin window, sometimes a thick beam pipe. Therefore we compare four cases, our idealized one without any material and with three steel window thicknesses of 0.1, 1 and 10 mm. This "window" was in the simulations a spherical iron (density $7.87\,\text{g/cm}^3$) shell of 40 cm radius, surrounding the point where the particles originated from. It can be seen that the thicker windows start to reduce the energy deposition only at large angles. At the forward angles the presence of material can even increase the energy deposition due to secondary interactions. As expected the material has more effect for the lower beam energy. Qualitatively the behaviour can be understood by looking at the particle spectra. These are shown in Fig. 4 for scattering angles of 10 ($\pm$ 5) degrees and 90 ($\pm$ 5) degrees. It can be seen that at 90 degrees the particle spectra are considerably softer than in the forward direction, which accounts for the larger effect of material. Of course also the spectra for the lower beam energy are softer than those from the higher one. A minimum ionizing particle would loose about 12 MeV/cm in iron, which already would cut into the spectrum. In fact all of the particles are on the $1/\beta^2$ part of the Bethe–Bloch equation, and therefore lose much more than 12 MeV/cm. And with decreasing energy this energy loss increases rapidly. So a 10 mm iron layer stops a significant fraction of the particles.

Two aspects should be kept in mind when interpreting these results:
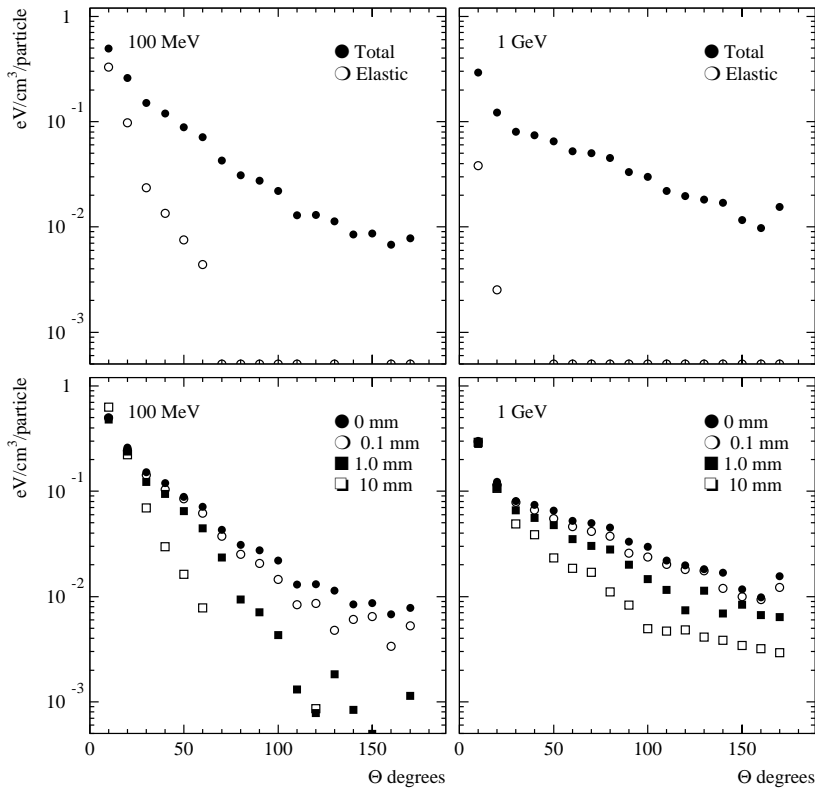
Fig. 3. Energy deposition in the polyethylene detectors as a function of angle with respect to the beam direction. Normalisation is to one particle incident on the $30\,\mu$m wire.

(i) At the low energies considered here evaporation fragments and splitting of the ^{12}C nucleus into three helium nuclei are important inelastic channels. The heavy fragments have not been transported. This underestimates the result and probably their effect would be to make the angular distribution flatter, since elastic scattering and particle production are less isotropic than evaporation and fragmentation. However, the heavy fragments are very slow and therefore highly ionising, so they most probably would be stopped in almost any kind of window separating the wire from the detectors.

(ii) As was pointed out previously the simulations should be done in a realistic geometry with realistic beam halo. Neither surrounding walls, nor support materials, nor the arriving beam have been included in the simulations. Their effect would be to generate stray radiation, mostly photons and neutrons all over the system. Especially plastic scintillators would be sensitive to this stray radiation field.
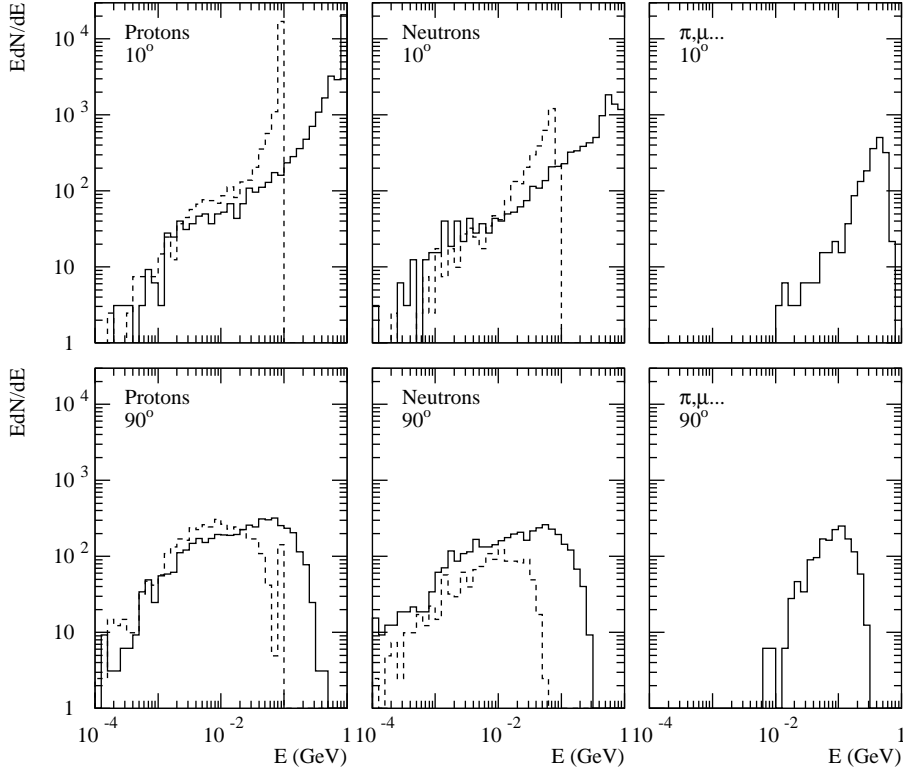
7

Fig. 4. Kinetic energy spectra of secondaries, the solid line shows the spectrum for a primary proton beam of 1 GeV kinetic energy and the dashed line for a primary proton beam of 100 MeV. Note that direct photons are not an important contribution and have not been plotted. The neutral pions however are included in the plots of the third column.

3 Beam heating of the wire

3.1 A simple model of heating

In the process of is interaction with the beam the wire the wire gets heated by energy absorption. We shall formulate a model to estimate the maximal temperature rise in the stationary situation when the wire sweeps back and forth with a given frequency. The formalism is generally valid for any particle type and any energy range. The numerical examples are given for a low energy proton beam. For a general discussion on heating in any obstacle by a primary beam we refer to [10], for a detailed discussion of the heating in a carbon wire by protons to [14] and for high energy electrons to [11]. We compile the main results here for convenience. Let us initially neglect conductive cooling and only consider radiative cooling, in the end of this section we will derive the

condition for this approximation.

When the wire is in the beam it is thus heated according to the equation

$$\frac{dT}{dt} = \frac{N\beta}{A\tau_0 c_V} \frac{dE}{dx} - \frac{2\sigma\eta T^4}{r c_V} \equiv a - bT^4 \quad, \tag{4}$$

and the maximal temperature it can reach is

$$T_m = \left(\frac{N\beta r}{2A\tau_0\sigma\eta} \frac{dE}{dx}\right)^{1/4} \quad. \tag{5}$$

For constant normalised emittance it is useful re-express everything in terms of β. Furthermore, we must also account for the fact that the highest temperature is reached in the part of the wire that sweeps through the centre of the assumed Gaussian beam profile. So all together we can write the maximum temperature as,

$$T_m^4 = \frac{4Nr}{4\pi \, \tau_0\sigma\eta} \frac{1}{\sqrt{\epsilon_{Nx}\epsilon_{Ny}\beta_{Tx}\beta_{Ty}}} \frac{\beta^2}{\sqrt{1 - \beta^2}} \frac{dE}{dz} \quad. \tag{6}$$

From the previous section we know that the energy deposited as heat in the wire is well described by the Bethe–Bloch formula. The asymptotic form of dE/dz for two ranges of β can be written as

$$\frac{dE}{dz} \sim \frac{1}{\beta^2}(\ln\beta + \text{const.}) \quad; \quad \text{for } \beta \ll 1 \quad, \tag{7}$$

$$\frac{dE}{dz} \sim \ln\frac{1}{1 - \beta^2} \quad; \quad \text{for } 1 - \beta^2 \ll 1 \quad. \tag{8}$$

We assume that β is not so small that dE/dz changes sign. The consequences for T_m in the limiting cases are

$$T_m \sim \ln\beta + \text{const.} \quad; \quad \text{for } \beta \ll 1 \quad, \tag{9}$$

$$T_m \sim (1 - \beta^2)^{-1/8}\left(\ln\frac{1}{1 - \beta^2}\right)^{1/4} \quad; \quad \text{for } 1 - \beta^2 \ll 1 \quad. \tag{10}$$

That is, for small β it goes to a constant up to logarithmic corrections, while at $\beta \lesssim 1$ the maximal temperature increases with the beam energy E like $T_m \sim E^{1/4}$. This estimate is valid for a wire which remains in the centre of the beam. If the wire is swept with a constant speed and frequency the time the wire spends in the beam decreases with increasing E since the beam size decreases, thus seemingly reducing the final temperature. In order to find out what really happens in that case we need to solve the dynamical heating problem.

9

3.2 Solution to the periodic heating

We shall now find the stationary temperature in the case the wire is swept through the beam with a given speed and frequency. The wire is cooled by radiation from a temperature T_0 to T_1 during the cooling time t_c, and then heated to T_2 during the heating time t_h. Putting $T_0 = T_2$ we shall find the maximal temperature in the stationary situation. During cooling the temperature is governed by the equation

$$\frac{dT}{dt} = -bT^4 \quad , \tag{11}$$

with the solution

$$T_1 = T_0 \left(\frac{1}{1 + 3bt_cT_0^3} \right)^{1/3} \equiv T_0\alpha(T_0) \quad . \tag{12}$$

We can interpret t_h as an effective heating time taking into account the variation of the beam intensity. After solving Eq. (4) and equating T_0 and T_2 we find the implicit equation for T_0

$$2 \left(\operatorname{atan}\frac{T_0}{T_m} - \operatorname{atan}\frac{T_0\alpha}{T_m} \right) + \ln \left[\frac{(T_m + T_0)(T_m - T_0\alpha)}{(T_m - T_0)(T_m + T_0\alpha)} \right] = 4bt_hT_m^3 \quad . \tag{13}$$

We can gain some insight by solving this equation in the limiting cases of very long and very short cooling times, i.e. $\alpha \simeq 0$ and $\alpha \simeq 1$.

3.2.1 Long cooling time

When the cooling time is long,

$$t_c \gg \frac{rc_V}{6\sigma\eta T_0^3} \quad , \tag{14}$$

i.e. $\alpha(T_0) \simeq 0$, Eq. (13) reduces to

$$2\operatorname{atan}\frac{T_0}{T_m} + \ln\frac{T_m + T_0}{T_m - T_0} = 4bt_hT_m^3 \quad , \tag{15}$$

which has the approximate solution

$$T_0 \simeq T_m \quad , \quad bt_hT_m^3 \gtrsim 1 \quad , \tag{16}$$
$$T_0 \simeq bt_hT_m^4 \quad , \quad bt_hT_m^3 \lesssim 1 \quad . \tag{17}$$

Using the effective heating time

$$t_h = \frac{2\Delta x}{v} = \frac{\sqrt{\epsilon_{Nx}\beta_{Tx}}}{v}\left(\frac{1-\beta^2}{\beta^2}\right)^{1/4} \quad , \tag{18}$$

we have in the limit of large and small beam energy

$$T_0 \simeq T_m \sim \text{const. since } bt_h T_m^3 \to \infty \quad \text{as } \beta \to 0 \quad , \tag{19}$$

$$T_0 \sim (1-\beta^2)^{1/8}\left(\ln\frac{1}{1-\beta^2}\right)^{1/4} \quad \text{since } bt_h T_m^3 \to 0 \quad \text{as } \beta \to 1 \quad . \tag{20}$$

In the case the final temperature is small it is necessary to pay extra attention to the condition in Eq. (14) since it tends to be more difficult to satisfy.

3.2.2   Short cooling time

It is also possible to find an approximative solution to Eq. (13) in the case the cooling time is very short. Then $\alpha \simeq 1$ and we also expect that $T_0 \simeq T_m$. Doing an expansion in small deviations we find

$$T_0 \simeq T_m\left(1 - \frac{2t_c}{rc_V}\frac{\sigma\eta T_m^3}{\exp[\frac{8\sigma\eta T_m^3 t_h}{rc_V}]-1}\right) \quad , \tag{21}$$

but, as we shall see, the cooling time has to be very short for this approximation to be valid.

3.2.3   Conductivity

So far we have neglected conductivity in the wire and we shall now estimate its importance compared to radiation. As a measure of the importance of conductivity we shall compare the radiated energy from the heated region of the wire with the conducted energy. The conducted energy per unit time is

$$P_c = -\pi r^2 \kappa \frac{\partial T}{\partial y}(0) = 2\pi r T_0^{5/2}\left(\frac{\eta\sigma\kappa r}{5}\right)^{1/2} \quad , \tag{22}$$

where

$$T(y) = T_0\left(1+\frac{y}{L}\right)^{-2/3} \quad , \quad L = \left(\frac{5r\kappa}{9\eta\sigma T_0^3}\right)^{1/2} \quad . \tag{23}$$

while the radiated power is

$$P_r = 4\pi r\Delta y\,\eta\sigma T_0^4 \quad . \tag{24}$$

11

The conductivity can be neglected when the condition

$$\frac{P_r}{P_c} = \frac{10\Delta y}{3L} = \left(\frac{5\eta\sigma T_0^3 \epsilon_{Ny}\beta_{Ty}}{r\kappa\beta\gamma}\right)^{1/2} \gg 1 \quad , \tag{25}$$

is satisfied.

3.3 Numerical example

In order to better see the validity of the approximations and the actual physical values they predict we shall go through a real example with a carbon wire in a proton beam. It is important to remember that the nature of our problem and the many approximations done in our derivation are such that we can't hope for high numerical precision results. The derived formulas can only give us an idea of the temperatures reached and show the temperatures energy dependence. The values we use in the Bethe–Bloch equation are given in Tab. 1. Other numerical values are given in Tab. 2.

With the parameters in the tables the maximal temperature is given by

$$T_m = 1200\,(1-\beta^2)^{-1/8}\left[\ln\frac{\beta^2}{1-\beta^2} + 9.47 - \beta^2\right]^{1/4} \text{ K} \quad . \tag{26}$$

In Fig. 5 the upper solid line shows T_m as a function of beam energy E using

$$\beta(E) = \sqrt{1 - \left(\frac{m_p c^2}{E + m_p c^2}\right)^2} \quad . \tag{27}$$

For long cooling time we can use the approximate formula in Eq. (16). It turns out that the combination $bt_h T_m^3$ is in fact small for a large range of energies so the approximate temperature is $T_0 = bt_h T_m^4$. We show this as a function of energy as the lower solid line in Fig. 5. The condition for the long cooling time to be valid is from Eq. (14) that

$$t_c \gg \frac{6\times10^7 \text{ K}^3}{T_0^3} \text{ s} \quad . \tag{28}$$

The right hand side of this equation is plotted as the solid line in Fig. 6.

For low energies the sweep frequency must be well below 0.01 Hertz for this approximation to be valid. The approximation of short cooling time is valid if the correction in Eq. (21) is small, which means

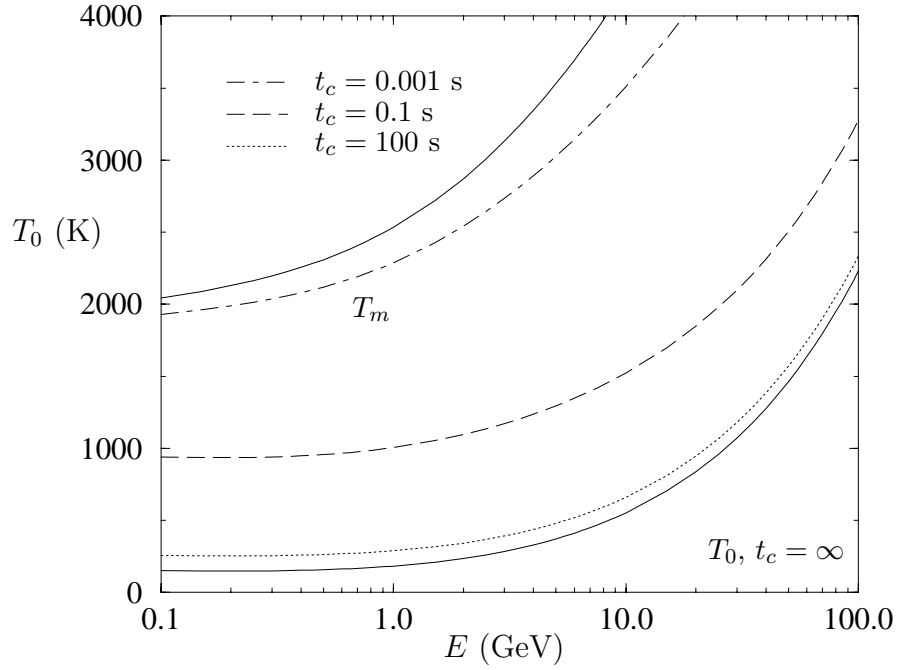$$t_c \ll \frac{rc_V}{2\sigma\eta T_m^3}(\exp[\frac{8\sigma\eta T_m^3 t_h}{rc_V}] - 1) \quad , \tag{29}$$

12

Fig. 5. Exact solution to Eq. (13) for several values of t_c. The upper solid line indicates T_m and the lower one is T_0 in the long cooling time approximation.
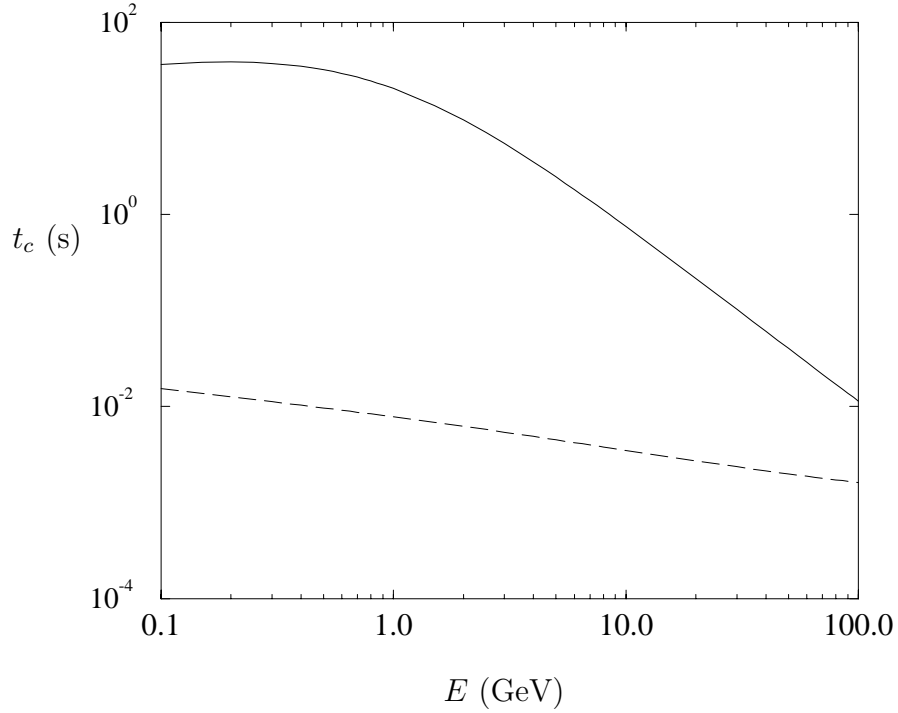

Fig. 6. The long cooling time approximation is valid when t_c is much larger than the values shown by the solid line above, while the short cooling time is valid far below the dashed line. There is thus a large interval where none of these approximations is valid.

13

and this limit is also plotted in Fig. 6 (dashed line). Since there is a wide range of cooling times for which none of the above approximations works we should also solve the full Eq. (13) exactly. This solution is presented in Fig. 5 for $t_c = 0.001$, 0.1 and 100 s.

Finally we need to check from Eq. (25) that the conductivity is negligible in our example. At high energy T_0 increases but at the same time Δy decreases, and the net effect is that the ratio P_r/P_c decreases. For the region in E that we have studied here we always have $P_r/P_c > 10$ which justifies neglecting conductivity.

4   Emittance blow-up of the primary beam

4.1   Emittance blow-up due to a thin window

The increase of the beam emittance when passing a thin window is a well understood process (see e.g. [13]). The scattering of the beam increases the angular spread of the beam which through filamentation results in an increased emittance

$$E = E_0 + \Delta E = E_0 + \frac{\pi}{2}\beta_T \langle \theta^2 \rangle. \tag{30}$$

Here E_0 is the initial emittance and β_T the Twiss value in the plane of the emittance at the thin window. The average square scattering angle will depend on the characteristics of the foil and the beam and is usually derived using formulas based on the Molière theory for multiple Coulomb scattering [15]. The emittance blow up due to the wire scanner device can be evaluated using the same formalism as the wire can be pictured as a virtual foil which thickness depends on the velocity and shape of the wire and the velocity of the beam. For the case of a wire with a circular cross section in a synchrotron with a revolution time of τ_0 (at $\beta = 1$) the virtual foil thickness (vft) can be written as

$$z_{vft} = \frac{(2r)^2 \pi \beta}{4v\tau_0} \quad . \tag{31}$$

4.2   Scattering theory

For small deflection angles a good approximation for the average root mean square scattering angle is given by [16,17]

$$\theta_0 = \frac{13.6 \text{ MeV}}{\beta pc} Q \sqrt{\frac{z}{X_0}} \left(1 + 0.038 \ln\left(\frac{z}{X_0}\right)\right), \tag{32}$$

14

where $p, \beta c$ and Q are momentum, velocity and charge number of the incident particles and $\frac{z}{X_0}$ is the thickness of the scattering medium in radiation lengths (z being the coordinate along the beam-line). However, the formula is only accurate to about 11% or better for $1\times10^{-3} < \frac{z}{X_0} < 100$. For a typical wire scanner with z_{vft} according to Eq. (31), $\frac{z_{vft}}{X_0}$ is much smaller than 1×10^{-3}. Consequently, we are for e.g. the CERN-CPS wire scanners left in a situation in between single Coulomb scattering and multiple scattering. We can get an idea of the order of magnitude if we assume that we are dealing with single Rutherford scattering events and that outside the atomic radius there is no interaction between the primary particle and the scattering centre. If for a numerical example we take the parameters in Tab. 2 at a kinetic proton beam energy of 1 GeV this approach gives a root mean square scattering angle of typically a few 1×10^{-11} radians while a multiple scattering approach using Eq. (32) yields a few 1×10^{-7} radians. The large range spanned by these two extreme approaches might be of theoretical interest but of no practical importance in a large physical beam emittance machine where both values yield an emittance blow-up well below the required precision. An attempt was done to measure the emittance blow-up in the CERN-CPS caused by the passage of a scanner wire using a two sweep process on a 500 ms flat-top of the magnetic cycle. An initial sweep and measurement was followed approximately 400 ms later by a back-sweep also with a measurement. The difference in emittance between the first and the second sweep was assumed to mainly be due to the blow-up in the wire. Earlier experience at the CPS has shown that this is a reasonable assumption. However, for a physical $\epsilon_h = 30\pi$ mm mrad proton beam at a beam energy of 300 MeV and a wire velocity of 20 m/s the *error* of the measured "emittance blow-up" was 0.3π mm mrad which is insuficient to separate between the two discussed approximations for the scattering process. Planned improvements, in line with findings presented in this note, for the dedicated low energy wire scanners in the PSB booster should make that possible.

5   Detection of secondary particles

In section 2 we have shown that a detectable amount of secondary particles are created by the primary beam when passing the wire of the fast wire scanners. A detector positioned at a given polar angle with respect to the beam direction can be used to monitor the number of particles scattered by the wire. If the angle is of the order of 10 degrees or larger, we know from section 2 that only nuclear scattering events, both elastic and inelastic, contribute.
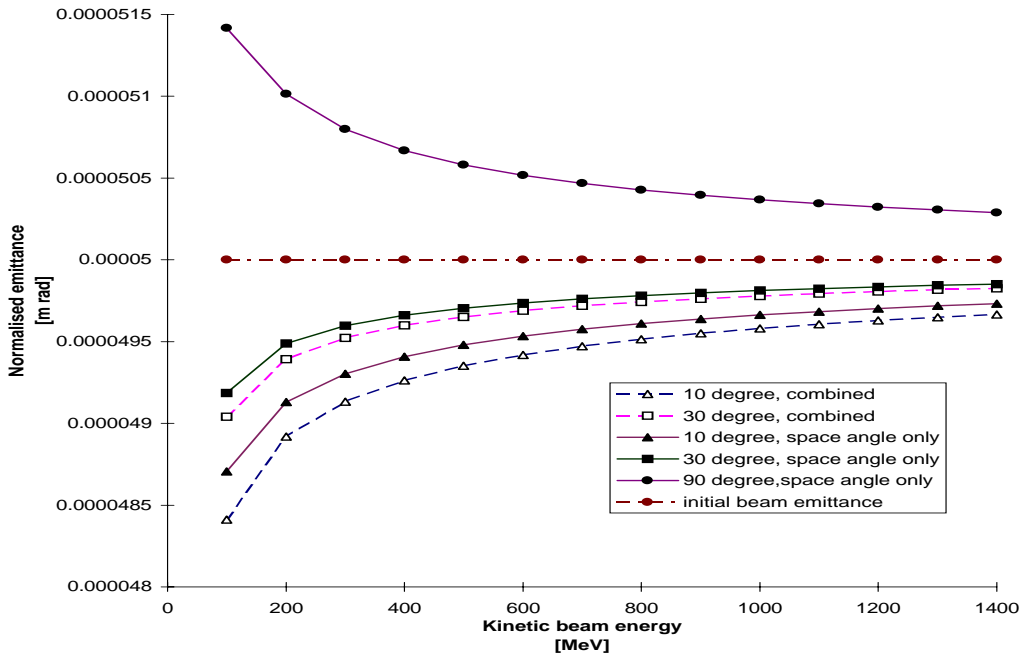
Fig. 7. The deduced emittance is deviating from the real beam emittance due to geometrical effects and the anisotropy of the induced particle shower. The effect is increasing with decreasing energy (larger transversal beam size). Both the combined result for both effects and the more significant geometrical effect are plotted for 10, 30 and 90 degree (only geometrical effects at 90 degree as the anisotropy effect of Eq. (33) is zero at 90 degree).

5.1 Effect on the deduced emittance

The detectors occupy a certain space-angle which together with other detector specific parameters determines the detection efficiency. For a beam which is large transversely such as the high intensity - low energy proton beam in the CPS, the space angle will change noticeably as the wire is passing through the beam.

The secondary particles will be emitted anisotropically with a majority of the particles going in the forward direction. This anisotropy will have "skewing" effect on the measured beam profile if the transverse beam size is large. For a rough estimate of the effect we will assume that the anisotropy is described by

$$W(\theta) = 1 + \cos\theta \tag{33}$$

A simple approach to calculate the size of the combined effect is to divide the beam into thin slices, calculate the detector efficiency and the resulting number

16

of detected particles for each slice and finally compare the initial emittance with the deduced emittance. Using the wire scanner example from Tab. 2 we have calculated the influence of the change in space angle and of the particle shower anisotropy for two wire scanner set-ups. In the first configuration the detector is positioned in the forward direction 15 cm from the wire at an angle of 30 degree to the beam axes and in the second configuration with an angle of 10 degree to the beam axes. The configuration with an angle of 30 degree to the beam axes is in the PS-complex enforced by the space limitations at the wire-scanner installations. In our numerical example the beam was initially assumed to be Gaussian and σ for the measured beam profile was calculated as

$$\sigma^2 = \frac{\sum\limits_{x=\text{first channel}}^{\text{last channel}} (x_i - \overline{x})^2 Ch(x_i)}{\sum\limits_{\text{last channel}}^{\text{first channel}} Ch(x_i)} \quad , \tag{34}$$

where

$$\overline{x} = \frac{\sum\limits_{x=\text{first channel}}^{\text{last channel}} x_i Ch(x_i)}{\sum\limits_{\text{last channel}}^{\text{first channel}} Ch(x_i)} \quad . \tag{35}$$

and where $Ch(x_i)$ is the number of counts in channel x_i.

In Fig. 7 we can see that the deviation form the real beam emittance is, as expected, increasing with decreasing beam energy. That is to say increasing with increasing transverse beam size. In Fig. 8 the measured beam profile during acceleration of the same beam at 100 MeV and 1.4 GeV are shown for a detector positioned at 85 degree angle to the beam axes. The beam is transversally larger at 100 MeV and the beam profile is slightly deformed due to the discussed geometrical effects. The resulting error in the deduced normalised emittance is small and will in most situations be insignificant. However, it is interesting to note that for the Gaussian beam shape the deformation of the beam profile is such that the influence on the deduced emittance goes from positive values for large angles to negative values for small angles.

5.2 Active sweep range of scanner

The large transverse size of the large emittance beam demand a long active sweep range for the scanner to i) establish the zero baseline and ii) avoid acquisition of "cut" profiles. At the CERN-CPS we have measured systematic differences of up to 10% between different wire scanners measuring the same beam but at different positions with different centres of the closed orbit. The
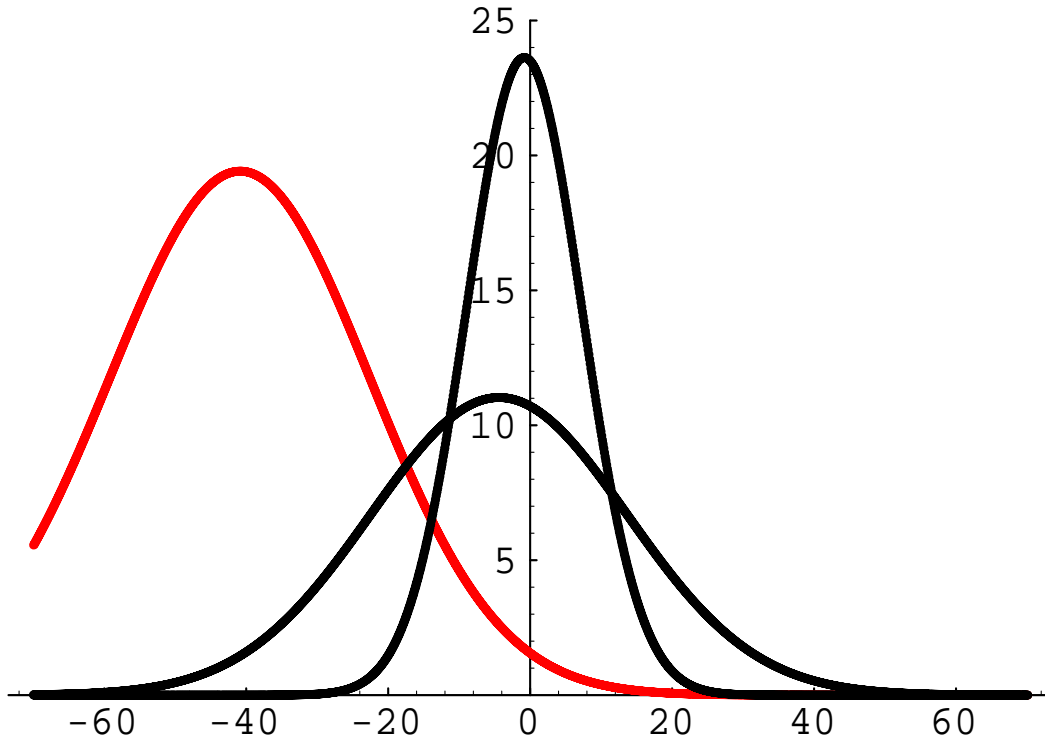
Fig. 8. In the centre of the figure the measured profiles for two beams with the same normalised emittance at two different energies, 100 MeV and 1.4 GeV, are shown. The wider profile at 100 MeV is slightly deformed due to geometrical effects. To the left in the figure a profile truncated at 2σ from the profile centre is shown. The wire scanner software will for this profile deduce an emittance which is 20% smaller than the true emittance.

numerical "simulations" discussed in the previous section confirms that such large deviations from the original beam emittance easily can be caused by a large offset of the centre of the profile. In Fig. 8 the measured beam profile at 100 MeV for a beam profile well centred in the wire-scanner sweep range and for one truncated at 2σ form the beam profile centre are shown. The presently used wire scanner software will for this profile deduce an emittance which is 20% smaller than the true beam emittance.

6   Discussion

We have presented new simulations for the creation of secondary particles in a thin carbon wire by a primary proton beam. The derived limits for the use of wire scanners show that the use of these devices in a low energy (50 MeV - 1 GeV) accelerators with large transverse beam size is fully feasible. The total deposited energy in the wire increases with decreasing beam energy. Nevertheless, the wire will not get hotter but rather the opposite due to the increase of the total heated wire volume as the beam size is usually large at

18

lower energies. The fact that a large beam can not be considered as a point source in relation to the detectors will only have small, and for most measurements, insignificant effect. The emittance blow-up will increase at lower energies but will for most practical purposes be of little importance. However, the large beam size requires a long active sweep range of the wire scanners to avoid cut-off effects which can result in significant deviations of the measured emittance from the true beam emittance.

7   Acknowledgements

References

[1] P. Lefèvre, *Mesure très peu destructive des distributions transversales dans le PS de 800 MeV à 26 GeV/c*, CERN internal note: CERN/PS/DL/Note 78-8.

[2] L.R. Evans and R. Shafer, *A carbon filament beam profile monitor for high energy proton- antiproton storage rings* in: The proceedings of the Workshop on intensity Limitations in Storage rings, Brookhaven National Laboratory, 1979.

[3] Ch. Steinbach and M. van Rooij, *A scanning wire beam profile monitor*, IEEE Trans. on Nucl. Sc. **NS-32**, 1985.

[4] A. Burns, J. Camas, E. D'amico, G. Ferioli, Q. King, K.H. Kissler, J. Mann and R. Schmidt, *Wire scanner news from the CERN-SPS* in: Proceedings of the Particle Accelerator Conference, Chicago, 1989.

[5] S. Hancock, M. Martini, M. van Rooij and Ch. Steinbach, *Experience with a fast wire scanner for beam profile measurements at the CERN PS* in: Proceedings of the Workshop on Advanced Beam Instrumentation, KEK, Tsukuba, Japan, 1991.

[6] K. Wittenburg, *Strahlprofilmonitore für den HERA-Protonenring*, DESY internal note: DESY HERA 1986-06

[7] K. Wittenburg, *Emittance Mesaurement in the Proton Accelerators at DESY* in: Proceedings of the International Workshop on Particle Dynamics in Accelerators, Tsukuba, Japan, 1994.

[8] V. Agoritsas, E. Falk, F. Hoekemeijer, J. Olsfors and Ch. Steinbach, *The fast wire scanners of the CERN PS*, CERN internal note: CERN/PS 95-06 (BD/OP).

[9] A. Fassò, A. Ferrari, J. Ranft and P. Sala, Proc IV Int. Conf. on Calorimetry in High Energy Physics, La Biodola, Sept. 20–25, 1993. Ed. A. Menzione and A. Scribano, World Scientific, p. 493 (1993).

[10] J. F. Janni, *Calculations of energy loss, range, pathlength, straggling, multiple scattering, and the probability of inelsatic nuclear collisions for 0.1-to 1000-MeV protons* US Air Force Weapons Laboratory report: AFWL-TR-65-150

[11] C. Fischer, R. Jung and J. Koopman, *Quartz wires versus carbon fibres for improved beam handling capacity of the LEP wire scanners* in: Proceedings of the Beam Instrumentation Workshop, Argonne, 1996.

[12] W. R. Leo, *Techniques for nuclear and particle physics experiments*, (Springer-Verlag, 1994).

[13] P. J. Bryant, *Beam transfer lines* in: Proceedings of the CERN Accelerator school, Fifth general accelerator physics course, Editor: S. Turner, Jyväskylä, Finland, 1992.

[14] P. Elmfors, A. Fasso, M. Huhtinen, M. Lindroos, J.Olsfors and U. Raich, *Wire scanners in Low energy accelerators*, CERN internal note: CERN/PS/OP Note 97-14

[15] H. A. Bethe, Phys. Rev. **89**, 1256 (1953).

[16] V. L. Highland, Nucl. Instr. and Meth. **129**, 497 (1979).

[17] G.R. Lynch and O.I. Dahl, Nucl. Instr. and Meth. **B58**, 6 (1991).